

# On Logical Extrapolation for Mazes with Recurrent and Implicit Networks

Brandon Knutson<sup>1</sup>, Amandin Chyba Rabeendran<sup>2</sup>, Michael Ivanitskiy<sup>1</sup>,  
Jordan Pettyjohn<sup>1</sup>, Cecilia Diniz Behn<sup>1</sup>, Samy Wu Fung<sup>1</sup>, Daniel McKenzie<sup>1</sup>,

<sup>1</sup>Department of Applied Mathematics and Statistics, Colorado School of Mines  
{bknutson, mivanits, jpettyjohn, cdinizbe, dmckenzie, swufung}@mines.edu

<sup>2</sup>Courant Institute of Mathematical Sciences, New York University  
atc9782@nyu.edu

## Abstract

Recent work suggests that certain neural network architectures—particularly recurrent neural networks (RNNs) and implicit neural networks (INNs)—are capable of logical extrapolation. When trained on easy instances of a task, these networks (henceforth: logical extrapolators) can generalize to more difficult instances. Previous research has hypothesized that logical extrapolators do so by learning a scalable, iterative algorithm for the given task which converges to the solution. We examine this idea more closely in the context of a single task: maze solving. By varying test data along multiple axes — not just maze size — we show that models introduced in prior work fail in a variety of ways, some expected and others less so. It remains uncertain whether any of these models has truly learned an algorithm. However, we provide evidence that a certain RNN has approximately learned a form of ‘deadend-filling’. We show that training these models on more diverse data addresses some failure modes but, paradoxically, does not improve logical extrapolation. We also analyze convergence behavior, and show that models explicitly trained to converge to a fixed point are likely to do so when extrapolating, while models that are not may exhibit more exotic limiting behavior such as limit cycles, *even when* they correctly solve the problem. Our results (i) show that logical extrapolation is not immune to the problem of *goal misgeneralization*, and (ii) suggest that analyzing the *dynamics* of extrapolation may yield insights into designing better logical extrapolators.

## 1 Introduction

A key feature of human learning is the ability to generalize from easy problem instances to harder ones, often by thinking for longer (Schwarzschild et al. 2021b). Work in multiple areas of machine learning has provided empirical evidence that neural networks are also capable of such *logical extrapolation* (also known as upwards generalization or algorithmic reasoning (Veličković et al. 2022)). Logical extrapolation is a form of out-of-distribution (OOD) generalization in which the test distribution is shifted away from the training distribution along an intuitively defined difficulty axis. These networks usually utilize *test-time scaling*, which increases their computational budget at test time to boost inference (Dehghani et al. 2018; Gilton, Ongie, and Willett 2021; Schwarzschild et al. 2021b; Bansal et al. 2022; Anil et al. 2022; OpenAI 2024; Geiping et al. 2025). In this work we conduct an in-depth

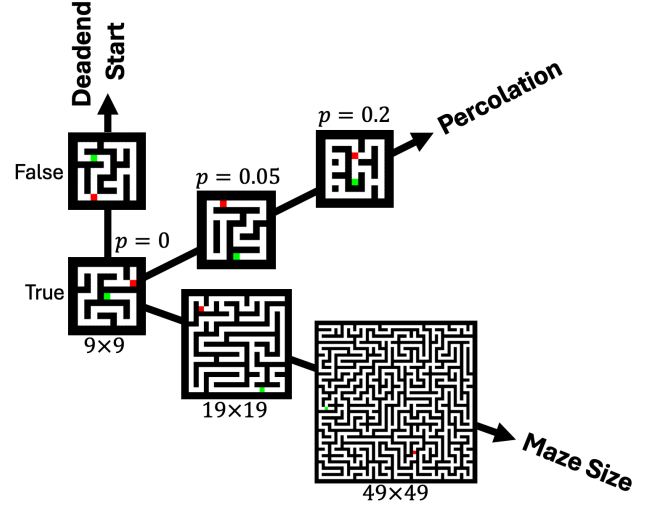


Figure 1: Three extrapolation dimensions: maze size, percolation, and deadend start. Each shown maze is generated using the indicated parameters. Green denotes the start position and red denotes the target.

study of logical extrapolation for two classes of neural networks that exhibit test-time scaling by iterating a recurrent block additional times: weight-tied RNNs and INNs, also known as Deep Equilibrium Networks (DEQs) (Bai, Kolter, and Koltun 2019; El Ghaoui et al. 2021; Wu Fung et al. 2022). We focus on a single task — maze-solving — a canonical spatial-reasoning task. We are interested in two intertwined questions:

- Q1 *Do RNNs and INNs learn an algorithm for maze-solving?*
- Q2 *Are the recurrent iterations converging to something? If yes, to what? Does this affect logical extrapolation in any way?*

We are motivated by various intriguing observations and partial results in the recent literature (Anil et al. 2022; Bansal et al. 2022; Schwarzschild et al. 2023, 2021b,c). Answering Q1 is necessary for assessing the robustness and trustworthiness of logical extrapolators, as we take “learn an algorithm” to mean “learn a correct and interpretable algorithm that scales to harder problems”. Q2 is important philosophically,

as many prior works explain the success of logical extrapolators by claiming that the recurrent part converges to a fixed point. While we confine our analysis to a single task, we suspect our insights will transfer to similar tasks.

To tackle Q1, we use the `maze-dataset` package (Ivanitskiy et al. 2023b,a). While previous studies on logical extrapolation in maze-solving have varied the test distribution by increasing maze size only, `maze-dataset` allows two new distribution shifts: (i) a variable `deadend_start`  $\in \{\text{True}, \text{False}\}$  which, when set to `True`, constrains the start point to have exactly one neighbor, and (ii) a percolation constant  $p \in [0, 1]$  which probabilistically determines the number of cycles in the maze. See Figure 1. Prior work (Bansal et al. 2022; Anil et al. 2022) has set `percolation` = 0 and `deadend_start` = `True` for both training and testing. By varying  $p$  and `deadend_start` we expose pretrained models (the RNN of (Bansal et al. 2022) and the INN of (Anil et al. 2022)) to corner cases not considered before. Examining how both models handle mazes containing cycles provides additional evidence that the RNN has learned a variant of the deadend-filling algorithm (Hendrawan 2020b), bolstering results of (Schwarzschild et al. 2023). However, by toggling the seemingly inconsequential `deadend_start` variable, we produce examples of mazes where deadend-filling would succeed, yet both models fail, suggesting that the RNN has *not* learned deadend-filling. Thus, our answer to Q1 is:

A1 *Partially. One RNN approximately learns deadend-filling — it succeeds like deadend-filling on acyclic mazes and fails like deadend-filling on mazes with cycles<sup>1</sup>. However, it also fails on mazes without a deadend start, revealing a mismatch. We trained many other models, but were unable to find clear-cut evidence of algorithm learning.*

While (Bansal et al. 2022) observes that, with proper training, RNNs converge to a fixed point even when extrapolating, the results of (Anil et al. 2022) hint at more complex behavior. Specifically, Anil et al. (2022, App. F, App. G) find evidence that RNNs may sometimes converge to limit cycles. To address Q2 rigorously, we quantify this phenomenon using tools from *Topological Data Analysis* (TDA) (De Silva, Skraba, and Vejdemo-Johansson 2012; Perea and Harer 2015; Tralie and Perea 2018). We find that, while the INN from (Anil et al. 2022) consistently converges to a fixed point, regardless of maze size, the RNN from (Bansal et al. 2022) exhibits more complex limiting behavior. To be correct, the iterative part of a logical extrapolator must converge into the pre-image of the solution after sufficient iterations. However, the exact convergence pattern inside the pre-image does not appear to matter — logical extrapolators that sometimes converge to limit cycles are as performant as extrapolators that always converge to fixed points. Thus, our answer to Q2 is:

A2 *Yes. Sometimes a fixed point, sometimes something more exotic. No, it doesn’t seem to matter.*

<sup>1</sup>Specifically, the output of the RNN agrees with deadend-filling on 98.8% of 143k tests mazes across a variety of sizes and percolation values.

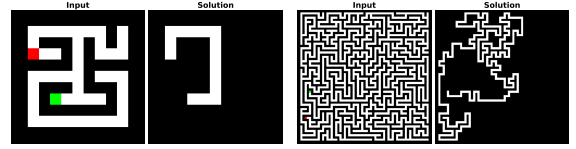


Figure 2: Maze input-solution pairs of size  $9 \times 9$  (left) and  $49 \times 49$  (right). Start positions are in **green** and end positions are in **red**. Mazes problems/inputs are RGB raster images and solutions are black and white images highlighting the solution path in white.

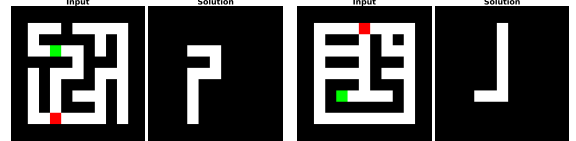


Figure 3: Example of maze with a start position that has multiple neighbors (left); example of a percolated maze (`percolation` = 0.2) with loops (right).

It is perhaps unsurprising that the pre-trained models we consider (Bansal et al. 2022; Anil et al. 2022) do not generalize to mazes with cycles, as they did not see such mazes in their training data. By retraining them using more diverse training data (i.e.,  $p > 0$ ) we investigate whether these models can be made more performant. We observe that a little bit goes a long way: if even a tiny fraction of training mazes contain cycles, performance is dramatically improved. We hypothesize that this may be because the models have learned to emulate a different maze solving algorithm—one which *does generalize* to mazes with cycles—although identifying this algorithm remains challenging.

## 2 Preliminaries and related works

### 2.1 The maze-solving task

In this and prior work (Schwarzschild et al. 2021a,b; Bansal et al. 2022; Anil et al. 2022), maze solving problems are encoded as raster images (Figure 2). Given this RGB input image, the task is to return a black and white image representing the unique path from start to end. We consider the “accuracy” of a model on a single maze to be 1 if its prediction is a valid path of minimal length and 0 otherwise. Instead of using the original “easy to hard” dataset (Schwarzschild et al. 2021a), we use the `maze-dataset` package (Ivanitskiy et al. 2023b) which provides the flexibility to modify the distribution from which (maze, solution) pairs are drawn. The original “easy to hard” dataset only contains acyclic (i.e. `percolation` = 0, any path between two nodes is unique) mazes generated via randomized depth-first search (RDFS) and with start positions having exactly degree 1 (i.e., `deadend_start`=`True`). We remove these restrictions to investigate the behavior of the selected models on out-of-distribution mazes in Section 2.1. More details on our usage of `maze-dataset` are given in Appendix Section A.

## 2.2 Recurrent neural networks

A special class of RNNs, namely, weight-tied input-injected networks (or simply weight-tied RNNs), are used in logical extrapolation (Schwarzschild et al. 2021b; Bansal et al. 2022). For a  $K$ -layer weight-tied RNN  $\mathcal{N}_\Theta$ , the output is given by

$$\begin{aligned} \mathcal{N}_\Theta(d) &= P_{\Theta_2}(u_K), \\ \text{where } u_j &= T_{\Theta_1}(u_{j-1}, d) \quad \text{for } j = 1, \dots, K. \end{aligned} \quad (1)$$

Here,  $\Theta_1$  and  $\Theta_2$  are the parameters of the networks  $T_{\Theta_1}$  and  $P_{\Theta_2}$  respectively, and  $\Theta := \{\Theta_1, \Theta_2\}$ , while  $d$  denotes the input features. These networks represent a unique class of architectures that leverage weight sharing across layers to reduce the number of parameters. The input injection at each layer ensures the network does not ‘forget’ the initial data (Bansal et al. 2022). In (Bansal et al. 2022), it is empirically observed that a certain weight-tied RNN extrapolates to larger mazes when applying more iterations. The authors speculate that the reason for this success is that the model has learned to converge to fixed points within its latent space (Section 7, (Bansal et al. 2022)).

## 2.3 Implicit networks

Drawing motivation from (Bansal et al. 2022), Anil et al. (2022) propose to use implicit neural networks (INNs) for logical extrapolation tasks. INNs are a broad class of architectures whose outputs are the fixed points of an operator parameterized by a neural network. That is,

$$\mathcal{N}_\Theta(d) = P_{\Theta_2}(u_\star) \quad \text{where} \quad u_\star = T_{\Theta_1}(u_\star, d). \quad (2)$$

Here again  $\Theta = \{\Theta_1, \Theta_2\}$  refers collectively to the parameters of the networks  $T_{\Theta_1}$  and  $P_{\Theta_2}$  and  $d$  is the input feature, while  $u_\star$  represents a fixed point of  $T_\Theta$ . These networks can be interpreted as infinite-depth weight-tied input-injected recurrent neural networks (El Ghaoui et al. 2021; Bai, Kolter, and Koltun 2019; Winston and Kolter 2020; Fung and Berkels 2024). Unlike traditional networks, INN outputs are not defined by a fixed number of computations but rather by an implicit condition. INNs have been applied to domains as diverse as image classification (Bai, Koltun, and Kolter 2020), inverse problems (Gilton, Ongie, and Willett 2021; Yin, McKenzie, and Fung 2022; Liu et al. 2022; Heaton et al. 2021; Heaton and Wu Fung 2023), optical flow estimation (Bai et al. 2022), game theory (McKenzie et al. 2024), and decision-focused learning (McKenzie, Wu Fung, and Heaton 2024). In principle, INNs are naturally suited for logical extrapolation tasks for which solutions can be characterized by a fixed point condition. Key to logical extrapolation is that this characterization is always the same, regardless of the difficulty of the problem at hand.

## 2.4 Topological data analysis in the latent space

For both RNNs and INNs, we call  $\{u_j\}_{j=1}^K \subset \mathbb{R}^n$  the *latent iterates*, and  $n$  the latent dimension. Note that  $n$  may be significantly larger than the output space dimension, so  $P_{\Theta_2}$  is a projection operator with large-dimensional fibers. Although models are trained to reduce loss (i.e. the discrepancy between  $\mathcal{N}_\Theta(d)$  and the true solution  $x^\star$ ) at every iteration (Bansal et al. 2022; Anil et al. 2022; Schwarzschild

et al. 2021b), there is no incentive for the iterative part of the network  $T_{\Theta_1}(\cdot, d)$  to prefer one element of the fiber  $P_{\Theta_2}^{-1}(x^\star) := \{u \in \mathbb{R}^n : P_{\Theta_2}(u) = x^\star\}$  over another, unless additional constraints are imposed upon  $T_{\Theta_1}$ , such as contractivity (El Ghaoui et al. 2021) or monotonicity (Winston and Kolter 2020). Thus,  $T_{\Theta_1}(\cdot, d)$  may exhibit more complex dynamics than convergence-to-a-point, while  $\mathcal{N}_\Theta(d)$  still yields the correct solution. Anil et al. (2022) proposed that, in order for  $T_{\Theta_1}(\cdot, d)$  to exhibit logical extrapolation<sup>2</sup>, it need not have a unique fixed point, but rather need only possess a global attractor. In other words, no matter which initialization  $u_0$  is selected, the latent iterates should exhibit the same asymptotic behaviour. They dub this property ‘path independence’. In (Anil et al. 2022, App. F, App. G) evidence is provided of instances  $d$  where the latent iterates induced by  $T_{\Theta_1}(\cdot, d)$  form a limit cycle, yet  $\mathcal{N}_\Theta(d)$  is correct.

If RNNs and INNs can generalize while converging to limit cycles, this has consequences for the design of logical extrapolators. For example, it is common practice to terminate the iteration when the residuals  $r_j := \|u_{j+1} - u_j\|_2$  drop below a certain tolerance. However, if the  $u_j$  have converged to a two-point cycle (see Figure 7) this condition will never be triggered. Thus, it is important to characterize the possible limiting behaviors of the sequence of latent iterates. To do so, we study its *shape* using topological data analysis (TDA) (De Silva, Skraba, and Vejdemo-Johansson 2012; Perea and Harer 2015; Tralie and Perea 2018). Following prior works using TDA to analyze periodicity (Perea and Harer 2015; Tralie and Perea 2018) we focus on the zeroth and first *persistent Betti numbers* — denoted as  $B_0$  and  $B_1$  respectively — of the point cloud  $\{u_j\}_{j=1}^K \subset \mathbb{R}^n$ . See Appendix Section B for precise definitions. TDA examines the shape of the object formed by the union of small balls centered at each  $u_j$ .  $B_0$  counts the number of connected components of this object, while  $B_1$  counts the number of loops which encircle a hole (Munch 2017). If the latent iterates have converged to a fixed point, then  $B_0 = 1, B_1 = 0$ , and this holds even if the convergence is only to within some small tolerance. If the latent iterates have converged to a limit cycle,  $B_1 > 0$ . By computing and interpreting  $B_0$  and  $B_1$  for a large number of input mazes, we identify three topologically distinct convergence behaviors.

## 3 Testing pre-trained models

We study two trained maze-solving models from previous works: an RNN from Bansal et al. (2022) which we call DT-Net, and an INN from Anil et al. (2022) which we call PI-Net<sup>3</sup>. While both works propose multiple models, we focus on the most performant model from each. Both DT-Net and PI-Net contain 0.78M parameters, facilitating fair comparison. DT-Net uses a progressive loss function to encourage improvements at each RNN layer. In this approach, the recurrent module is run for a random number of iterations, and the resulting output is used as the initial

<sup>2</sup>Note they call this property ‘upwards generalization’.

<sup>3</sup>PI-Net stands for ‘Path-Independent’ net, as path independence is a feature identified in (Anil et al. 2022) as being strongly correlated with generalization.

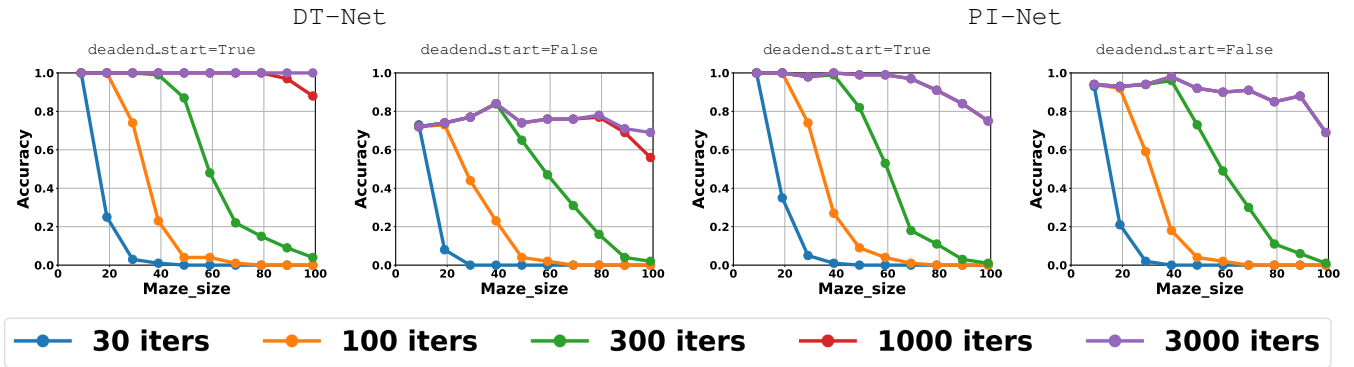


Figure 4: **Left:** DT-Net extrapolation accuracy (see Section 2.1) at various maze sizes, with `deadend.start=True` and `deadend.start=False`. **Right:** Analogous results for PI-Net. Both models extrapolate well to larger mazes given sufficient iterations. However, performance diminishes when the start position is allowed to have neighbors, regardless of the number of iterations. The sample size was limited to 100 mazes due to hours of compute time required for large  $99 \times 99$  mazes.

input for the RNN, while gradients from the initial iterations are discarded. The model is then trained to produce the solution after another random number of iterations. We refer the reader to (Bansal et al. 2022, Section 3.2) for additional details. For PI-Net, path-independence is encouraged in two ways: (i) by using random initialization for half of the batch and zero initialization for the other half, and (ii) by varying the compute budgets/depths of the forward solver during training.

### 3.1 Distribution shift

Using maze-dataset we explore the out-of-distribution behavior of DT-Net and PI-Net. As shown in Figure 1 we vary the distribution along three dimensions: increasing maze size, setting `deadend.start` to false, and increasing percolation.

**Maze size.** We first verify the extrapolation performance of DT-Net and PI-Net with increasing maze size. For each maze size  $n \times n$ , where  $n \in \{9, 19, 29, \dots, 99\}$ , we tested each model on 100 mazes. As expected, with sufficient iterations, both models achieve strong performance, confirming the results of (Bansal et al. 2022; Anil et al. 2022). See the plots labeled `deadend.start=True` in Figure 4. Both models achieve perfect accuracy on the  $9 \times 9$  mazes of the training distribution. Furthermore, with 3,000 iterations, DT-Net achieves perfect accuracy and correctly solved all test mazes. PI-Net achieved near perfect accuracy on smaller mazes, but performance diminished for mazes larger than  $59 \times 59$ . Importantly, running more iterations usually helps and never harms accuracy. Note that for PI-Net the performance of the model after 1,000 iterations is identical to performance after 3,000 iterations at all tested maze sizes, suggesting that convergence occurred by 1,000 iterations.

**Deadend start.** Allowing the start position to have multiple neighbors, i.e., setting `deadend.start` to `False`, represents a different out-of-distribution shift from the training dataset. This shift diminishes the performance of both models. See the plots labeled `deadend.start=False` in Figure 4.

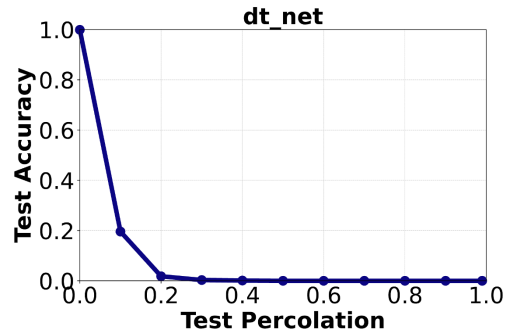


Figure 5: The accuracy of DT-Net rapidly diminishes when percolation increases above 0. DT-Net was iterated 30 times, and the resulting outputs do not change with additional iterations. The corresponding plot for PI-Net is nearly identical.

With this shift, accuracy on  $9 \times 9$  mazes drops from 1.00 to 0.72 for DT-Net and from 1.00 to 0.94 for PI-Net. Interestingly, the fraction of failed predictions remains relatively stable as maze size is increased. There is no clear qualitative difference between mazes that were correctly and incorrectly solved by the models. Both models correctly solve some instances where the start position has multiple neighbors (see Appendix Figure 12). However, we do observe that accuracy decreases monotonically as the degree of the start node increases. There is no discernible pattern to the models’ failures; sometimes they are only one or two pixels away from the correct solution, sometimes they are missing large chunks of the correct path (see Appendix Section D.1).

**Percolation.** The final out-of-distribution shift we consider is increasing the percolation value of the test dataset from 0. We reiterate that when percolation equals 0, all mazes are acyclic. Increasing percolation adds cycles to the maze, introducing multiple solutions where there was previously exactly one. This shift significantly reduces accuracy, as shown in Figure 5. Notably, increasing the number of iterations beyond 30 in this setting *does not improve model performance*.



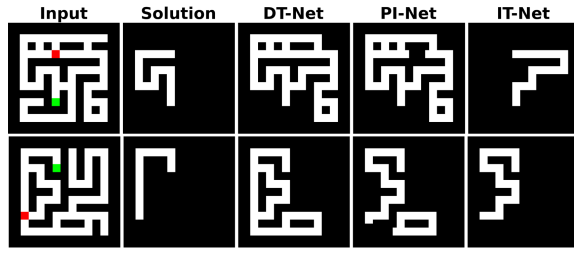


Figure 6: Two examples of mazes with cycles. DT-Net fails like deadend-filling by retaining cycles from the input in its prediction. PI-Net approximates deadend-filling but with some segments of white pixels removed. In the first example (top row), IT-Net predicts a minimal path (length 9) that is different from the solution (length 9); in the second example (bottom row), IT-Net predicts a valid non-minimal path (length 11) that is longer than the solution (length 8).

### 3.2 Latent dynamics

In (Anil et al. 2022, App. F, App. G) evidence of instances  $d$  where the latent iterates induced by  $T_{\Theta_1}(\cdot, d)$  form a limit cycle, yet  $\mathcal{N}_{\Theta}(d)$  is correct, is provided. Specifically, the residuals  $r_j := \|u_{j+1} - u_j\|_2$ , i.e. the distances between consecutive iterates, are considered. If  $r_j = 0$  for all sufficiently large  $j$  then the  $u_j$  have converged to a fixed point. However, (Anil et al. 2022) finds maze instances  $d$  such that the residual sequence  $\{r_j\}_{j=\tilde{K}}^K$  induced by a variant<sup>4</sup> of PI-Net is visually periodic.

We investigate the limiting behavior of PI-Net and DT-Net further. For both models, we consider 100  $n \times n$  mazes where  $n = 9, 19, \dots, 69$ . We set `percolation` = 0 and `deadend.start` = True. We select a “burn-in” parameter  $\tilde{K} < K$  and then consider latent iterates  $\{u_j\}_{j=\tilde{K}}^K$ . We set  $\tilde{K} = 3,001$  and  $K = 3,400$ . We observe periodicity of residuals for DT-Net (see Figure 7, third panel) and discover a novel asymptotic behavior of the residuals: convergence to a *nonzero value* (see Figure 7, panel 1). To explain both behaviors further, we introduce two tools.

**PCA.** Projecting the high-dimensional latent iterates onto their first three principal components provides a glimpse into the underlying geometry of  $\{u_j\}_{j=\tilde{K}}^K$  responsible for the observed residual sequences. We identify a sequence of latent iterates for DT-Net that oscillates between two points (see Figure 7, panel 2), yielding constant, non-zero, values of  $r_j$  equal to the distance between these points. We call such limiting behavior a *two-point cycle*. We also identify a sequence of latent iterates for DT-Net that oscillates between two loops (see Figure 7, panel 4), yielding values of  $r_j$  that oscillate around the (non-zero) distance between these loops. We call such limiting behavior a *two-loop cycle*. To the best of our knowledge, neither of these limiting behaviors has been observed previously in the latent dynamics of a logical extrapolator.

**TDA.** To quantify the frequency with which these limiting

<sup>4</sup>Although not the variant we consider, see Appendix Section C.3 for further discussion.

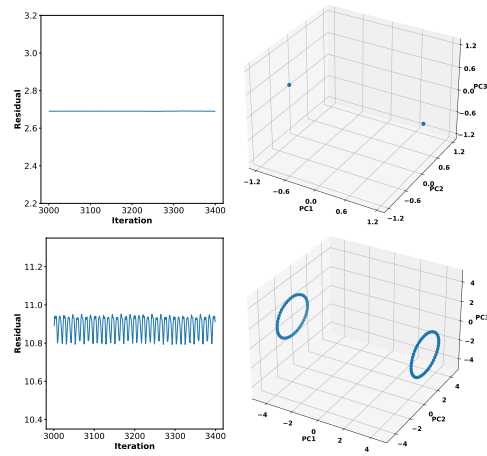


Figure 7: Residual plots and corresponding PCA projections for two sequences of DT-Net latent iterates. The left two plots indicate oscillation between two points corresponding to  $[B_0, B_1] = [2, 0]$  for a  $19 \times 19$  maze. The right two plots indicate oscillation between two loops corresponding to  $[B_0, B_1] = [2, 2]$  for a  $69 \times 69$  maze. Both mazes were solved correctly.

behaviors occur, we use TDA (see Section 2.4). This is possible because these limiting behaviors are distinguishable using the zeroth ( $B_0$ ) and first ( $B_1$ ) persistent Betti numbers (see Section 2.4 and Appendix Section B). Convergence to a point is associated to  $[B_0, B_1] = [1, 0]$ , a two-point cycle is associated to  $[B_0, B_1] = [2, 0]$ , while a two-loop cycle yields  $[B_0, B_1] = [2, 2]$ . Table 1 summarizes the TDA results.

For PI-Net, every latent sequence converges to a fixed-point. For DT-Net at every maze size the majority of latent sequences approach a two-point cycle, a minority approach a two-loop cycle, and a few approach some other geometry. We find no correlation between limiting behaviour and accuracy. DT-Net, when given 3000+ iterations, achieves perfect accuracy (see Figure 4, panel 1) even though, for a majority of larger mazes, it converges to a two-point or two-loop cycle. On the other hand, although PI-Net converges to a fixed point for all  $69 \times 69$  mazes we tested, it does not achieve perfect accuracy (see Figure 4, panel 3).

## 4 The effect of diversifying training data

It is well known that increasing the size of the training dataset improves model generalization (Kaplan et al. 2020). More recent works have also highlighted the importance of training dataset diversity and difficulty for generalization (Rolf et al. 2021; Andreassen et al. 2022). In Section 3 we identified the failure of DT-Net and PI-Net to generalize to mazes with loops. We attempt to address this by training new models on diversified data containing some mazes with loops. We again use DT-Net but replace PI-Net with a simpler implicit network we call IT-Net.<sup>5</sup> We also train and test

<sup>5</sup>Although the pretrained model and associated code from (Anil et al. 2022) is publicly available and suitable for inference, we encountered difficulties adapting the original implementation for

MODEL	$[B_0, B_1]$	$n$ for $n \times n$ maze					
		9	19	29	39	49	59
DT-Net	$[1, 0]^*$	15	0	0	0	0	0
	$[1, 1]$	6	6	0	0	0	0
	$[2, 0]$	79	88	95	100	98	98
	$[2, 1]$	0	1	0	0	0	0
	$[2, 2]$	0	5	5	0	2	2
PI-Net	$[1, 0]^*$	100	100	100	100	100	100
IT-Net	$[1, 0]^*$	100	100	100	100	100	100

Table 1: Betti number frequencies for DT-Net and PI-Net. PI-Net always exhibits fixed-point convergence ( $[B_0, B_1] = [1, 0]$ ) whereas DT-Net usually approach a two-point cycle ( $[B_0, B_1] = [2, 0]$ ) or sometimes a two-loop cycle ( $[B_0, B_1] = [2, 2]$ ). \*Sequence converged to within 0.01.

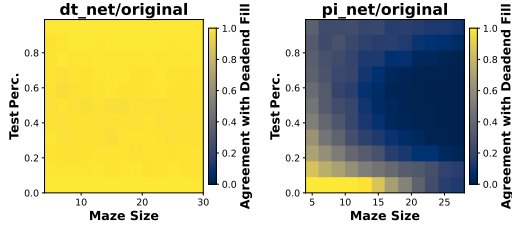


Figure 8: Agreement of pretrained DT-Net and PI-Net with deadend-fill algorithm, across 143K mazes with various size and percolation values. A value of 1.0 (yellow) means predictions perfectly coincide with deadend-filling algorithm, even when incorrect. DT-Net shows near perfect agreement, whereas PI-Net predictions were often qualitatively similar but different by multiple pixels, resulting in low agreement.

a model called FF-Net, a fully-convolutional feedforward network with a fixed depth of 30 layers, which serves as a baseline for generalization performance. Unlike DT-Net and IT-Net, FF-Net is incapable of test-time scaling. FF-Net is not weight-tied and so has roughly  $10\times$  more weights than IT-Net. To diversify the training data we keep maze size fixed at  $9 \times 9$  while varying the percolation value. Then, we train randomly-initialized instances of DT-Net and IT-Net. We evaluate these models on test data with varying maze size and percolation value; see Figure 9. For more training details, see Appendix Section C.2.

**Results** Increasing percolation shifts the training distribution closer to that of most test mazes. Thus the observed increase in overall test accuracy shown in Figure 9 and Ap-

pendix Figure 14 is expected. We note the surprising jump in overall test accuracy—particularly for DT-Net—in response to a very small increase in percolation from 0 to 0.010. We interpret this switching behavior as a possible indication that diversification induces DT-Net to emulate a different class of algorithms capable of solving mazes with loops. However, this emulation is only approximate. Figure 9 shows that although the overall accuracy of both models increases as  $p$  increases, their ability to extrapolate to larger mazes diminishes. We could not identify a clear pattern in  $(n, p)$  values for which these models succeed, other than that performance degrades as the test distribution moves away from the training distribution. Consequently, it is hard to say with confidence that any of these models are behaving algorithmically.

DT-Net and IT-Net have different architectures and were trained with different techniques. And yet Figure 9 and Appendix Figure 14 show that both models generalize nearly equally well. This suggests that generalization is more sensitive to the diversity of the training dataset than the choice of model. Nonetheless, the results indicate specific models may be more suited for different extrapolation directions. Figure 9 shows DT-Net trained with percolation = 0 perfectly solves larger mazes despite only seeing  $9 \times 9$  mazes in training, and IT-Net trained with percolation = 0 solves mazes with cycles better than the other models despite never seeing cycles in training.

DT-Net and IT-Net have different architectures and were trained with different techniques. And yet Figure 9 and Appendix Figure 14 show that both models generalize nearly equally well. This suggests that generalization is more sensitive to the diversity of the training dataset than the choice of model. Nonetheless, the results indicate specific models may be more suited for different extrapolation directions. Figure 9 shows DT-Net trained with percolation = 0 perfectly solves larger mazes despite only seeing  $9 \times 9$  mazes in training, and IT-Net trained with percolation = 0 solves mazes with cycles better than the other models despite never seeing cycles in training.

## 5 Have these networks learned an algorithm?

In analyzing the failures of the pretrained DT-Net on mazes with cycles (see Figure 6) and `deadend_start=True` we observed that the cycles remain part of the output. This is characteristic of the deadend-filling algorithm (Hendrawan 2020a) for maze solving. To study this further, we implemented deadend-filling, generated a large dataset (143k) of mazes with varying percolation and size, and compared the outputs of DT-Net to deadend-filling on these mazes. Our analysis reveals that DT-Net matches the output of deadend-filling — succeeding when deadend-filling succeeds, yielding the same incorrect output when deadend-filling fails — 98.8% of the time (see Figure 8). It appears that DT-Net has indeed learned to emulate<sup>6</sup> deadend-filling, at least when `deadend_start=True`.

The situation with the pretrained PI-Net is less clear. As shown in Figure 8, PI-Net has low agreement with deadend-filling. However, a closer examination of PI-Net predictions reveals that the disagreement with deadend-filling is often very minor. PI-Net predictions are usually qualitatively very similar to deadend-filling. But for mazes that are large or contain many cycles, PI-Net predictions match deadend-filling but with some segments of white pixels removed (see Figure 6), causing a low agreement. This slight difference with deadend-filling causes the disagreement shown in Fig-

<sup>6</sup>We use the word ‘emulate’ to describe this form of agreement between a logical extrapolator and an algorithm. A stronger form of agreement is to match the iterates of the logical extrapolator to the iterates of the algorithm (Veličković et al. 2022). Some evidence that DT-Net and deadend-filling agree in this stronger sense is provided in (Schwarzschild et al. 2023).

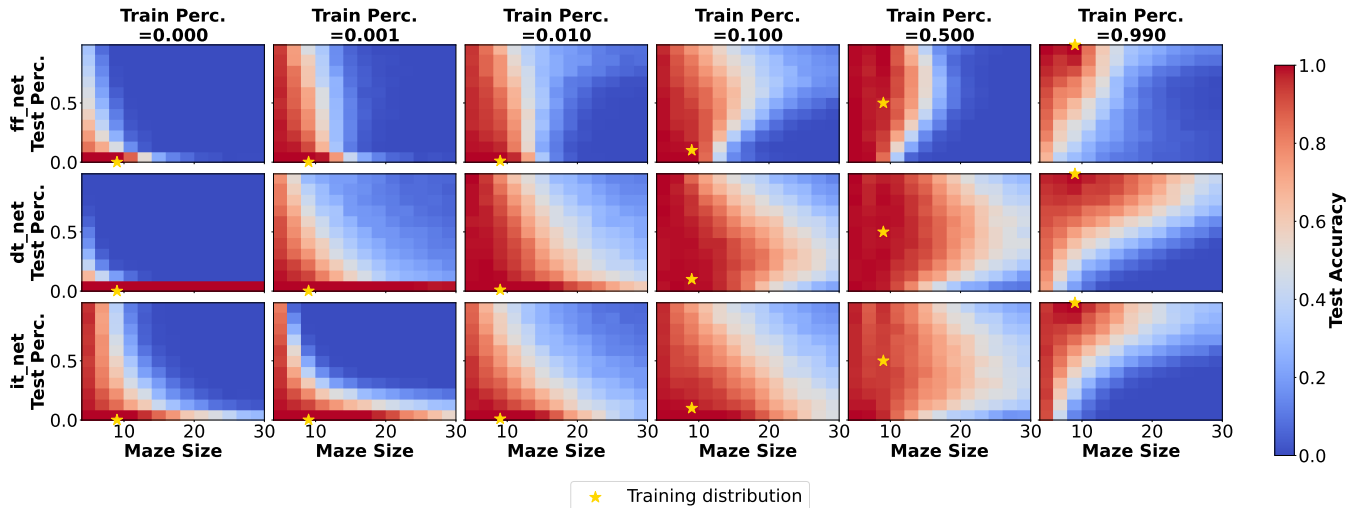


Figure 9: Heatmaps of test accuracy for FF-Net (top row), DT-Net (middle row) and IT-Net (bottom row) across various test maze sizes and test percolation values. A slight increase to training percolation (i.e. moving the gold star up) causes a dramatic increase in overall test accuracy. Each cell corresponds to 1,000 sampled test mazes.

ure 8 and suggests that PI-Net also has learned to approximate deadend-fill, but less successfully.

The models trained on diversified data showed superior overall accuracy (see Figure 9) but worse logical extrapolation performance. Further, their predictions were less qualitatively consistent and thus difficult to identify with an algorithm.

## 6 Limitations

One limitation of our work is that we limit ourselves to a single task. We focus on maze solving because it offers a variety of relatively intuitive distributional shifts (see Figure 1). It would be interesting to apply our approach to other logical extrapolation tasks. A second, more philosophical weakness relates to what it means to ‘learn an algorithm’, and what shifts of the test distribution should be considered reasonable.

## 7 Discussion and Conclusion

We present an in-depth look into logical extrapolation for a particular task: maze-solving. We confirm that by increasing the test-time compute budget (i.e., the number of iterations) certain models can solve much larger mazes than those in the training data, an impressive feat of OOD generalization. However, these models fail in interesting ways when the test distribution is shifted along other axes of difficulty. The observed failure modes indicate that logical extrapolators sometimes behave algorithmically, and we present evidence that DT-Net (Bansal et al. 2022) has indeed learned to emulate a simple algorithm for maze-solving, deadend-filling. As deadend-filling is known to fail on mazes with cycles, this also suggests that goal misgeneralization (Shah et al. 2022; Langosco et al. 2022) may be the cause of the observed failures. Perhaps logical extrapolators are learning the simplest algorithm which fits the training data?

However, our experiments with training data diversification show that getting a neural network to learn an algorithm is a challenging task. Although adding mazes with cycles to the training data boosts model performance, the resulting models do not appear to behave algorithmically, and their ability to extrapolate to larger mazes is diminished. Moreover, we show that logical extrapolators can succeed even when their iterative part does not converge to a fixed point, and identify and quantify two exotic limiting behaviors. This complicates the view of logical extrapolators as fixed-point-finding routines (Bansal et al. 2022). This also has consequences for training techniques which assume convergence to a fixed point (Wu Fung et al. 2022; Geng et al. 2021b,a; Ramzi et al. 2022).

To conclude, although there does appear to be something special about logical extrapolation, the usual caveats about OOD generalization still apply. Logical extrapolators may appear to behave algorithmically when the variation of the test distribution is tightly controlled, but respond in unexpected ways to other distribution shifts, much like other neural networks (Darestani, Chaudhari, and Heckel 2021; Gottschling et al. 2025; Heckel et al. 2024). Future work should focus on identifying conditions under which reliable algorithm learning is possible or reliable, and further exploring the relation of latent dynamics with logical extrapolation.

## Acknowledgments

This work was supported by the National Science Foundation under Grant DMS-2309810.

## References

- Andreassen, A. J.; Bahri, Y.; Neyshabur, B.; and Roelofs, R. 2022. The Evolution of Out-of-Distribution Robustness Throughout Fine-Tuning. *Transactions on Machine Learning Research*.
- Anil, C.; Pokle, A.; Liang, K.; Treutlein, J.; Wu, Y.; Bai, S.; Kolter,

- J. Z.; and Grosse, R. B. 2022. Path Independent Equilibrium Models Can Better Exploit Test-Time Computation. In Koyejo, S.; Mohamed, S.; Agarwal, A.; Belgrave, D.; Cho, K.; and Oh, A., eds., *Advances in Neural Information Processing Systems*, volume 35, 7796–7809. Curran Associates, Inc.
- Bai, S.; Geng, Z.; Savani, Y.; and Kolter, J. Z. 2022. Deep equilibrium optical flow estimation. In *Proceedings of the IEEE/CVF conference on computer vision and pattern recognition*, 620–630.
- Bai, S.; Kolter, J. Z.; and Koltun, V. 2019. Deep Equilibrium Models. *Advances in Neural Information Processing Systems*, 32.
- Bai, S.; Koltun, V.; and Kolter, J. Z. 2020. Multiscale Deep Equilibrium Models. *Advances in Neural Information Processing Systems*, 33: 5238–5250.
- Bansal, A.; Schwarzschild, A.; Borgnia, E.; Emam, Z.; Huang, F.; Goldblum, M.; and Goldstein, T. 2022. End-to-end Algorithm Synthesis with Recurrent Networks: Extrapolation without Overthinking. In Koyejo, S.; Mohamed, S.; Agarwal, A.; Belgrave, D.; Cho, K.; and Oh, A., eds., *Advances in Neural Information Processing Systems*, volume 35, 20232–20242. Curran Associates, Inc.
- Darestani, M. Z.; Chaudhari, A. S.; and Heckel, R. 2021. Measuring robustness in deep learning based compressive sensing. In *International Conference on Machine Learning*, 2433–2444. PMLR.
- De Silva, V.; Skraba, P.; and Vejdemo-Johansson, M. 2012. Topological Analysis of Recurrent Systems. In *NIPS 2012 Workshop on Algebraic Topology and Machine Learning, December 8th, Lake Tahoe, Nevada*, 1–5.
- Dehghani, M.; Gouws, S.; Vinyals, O.; Uszkoreit, J.; and Kaiser, L. 2018. Universal transformers. *arXiv preprint arXiv:1807.03819*.
- El Ghaoui, L.; Gu, F.; Travacca, B.; Askari, A.; and Tsai, A. 2021. Implicit Deep Learning. *SIAM Journal on Mathematics of Data Science*, 3(3): 930–958.
- Fung, S. W.; and Berkels, B. 2024. A Generalization Bound for a Family of Implicit Networks. *arXiv preprint arXiv:2410.07427*.
- Geiping, J.; McLeish, S.; Jain, N.; Kirchenbauer, J.; Singh, S.; Bartoldson, B. R.; Kailkhura, B.; Bhatele, A.; and Goldstein, T. 2025. Scaling up Test-Time Compute with Latent Reasoning: A Recurrent Depth Approach. *arXiv preprint arXiv:2502.05171*.
- Geng, Z.; Guo, M.-H.; Chen, H.; Li, X.; Wei, K.; and Lin, Z. 2021a. Is Attention Better Than Matrix Decomposition? In *International Conference on Learning Representations*.
- Geng, Z.; Zhang, X.-Y.; Bai, S.; Wang, Y.; and Lin, Z. 2021b. On Training Implicit Models. *Advances in Neural Information Processing Systems*, 34: 24247–24260.
- Gilton, D.; Ongie, G.; and Willett, R. 2021. Deep Equilibrium Architectures for Inverse Problems in Imaging. *IEEE Transactions on Computational Imaging*, 7: 1123–1133.
- Gottschling, N. M.; Antun, V.; Hansen, A. C.; and Adcock, B. 2025. The Troublesome Kernel: On Hallucinations, No Free Lunches, and the Accuracy-Stability Tradeoff in Inverse Problems. *SIAM Review*, 67(1): 73–104.
- Hatcher, A. 2002. *Algebraic Topology*. Cambridge University Press.
- Heaton, H.; and Wu Fung, S. 2023. Explainable AI via learning to optimize. *Scientific Reports*, 13(1): 10103.
- Heaton, H.; Wu Fung, S.; Gibali, A.; and Yin, W. 2021. Feasibility-based fixed point networks. *Fixed Point Theory and Algorithms for Sciences and Engineering*, 2021: 1–19.
- Heckel, R.; Jacob, M.; Chaudhari, A.; Perlman, O.; and Shimron, E. 2024. Deep learning for accelerated and robust MRI reconstruction. *Magnetic Resonance Materials in Physics, Biology and Medicine*, 37(3): 335–368.
- Hendrawan, Y. 2020a. Comparison of Hand Follower and Dead-End Filler Algorithm in Solving Perfect Mazes. In *Journal of Physics: Conference Series*, volume 1569, 022059. IOP Publishing.
- Hendrawan, Y. F. 2020b. Comparison of Hand Follower and Dead-End Filler Algorithm in Solving Perfect Mazes. *Journal of Physics: Conference Series*, 1569(2): 022059.
- Ivanitskiy, M. I.; Sandoval, A.; Knutson, B.; and Spies, A. F. 2023a. Maze Dataset. <https://github.com/understanding-search/maze-dataset>. Accessed: 2025-05-02.
- Ivanitskiy, M. I.; Shah, R.; Spies, A. F.; Räuker, T.; Valentine, D.; Rager, C.; Quirke, L.; Mathwin, C.; Corlouer, G.; Behn, C. D.; and Fung, S. W. 2023b. A Configurable Library for Generating and Manipulating Maze Datasets. *arXiv:2309.10498*.
- Kaplan, J.; McCandlish, S.; Henighan, T.; Brown, T. B.; Chess, B.; Child, R.; Gray, S.; Radford, A.; Wu, J.; and Amodei, D. 2020. Scaling Laws for Neural Language Models. *arXiv:2001.08361*.
- Langosco, L. L. D.; Koch, J.; Sharkey, L. D.; Pfau, J.; and Krueger, D. 2022. Goal Misgeneralization in Deep Reinforcement Learning. In Chaudhuri, K.; Jegelka, S.; Song, L.; Szepesvari, C.; Niu, G.; and Sabato, S., eds., *Proceedings of the 39th International Conference on Machine Learning*, volume 162 of *Proceedings of Machine Learning Research*, 12004–12019. PMLR.
- Liu, J.; Xu, X.; Gan, W.; Kamilov, U.; et al. 2022. Online deep equilibrium learning for regularization by denoising. *Advances in Neural Information Processing Systems*, 35: 25363–25376.
- McKenzie, D.; Heaton, H.; Li, Q.; Wu Fung, S.; Osher, S.; and Yin, W. 2024. Three-Operator Splitting for Learning to Predict Equilibria in Convex Games. *SIAM Journal on Mathematics of Data Science*, 6(3): 627–648.
- McKenzie, D.; Wu Fung, S.; and Heaton, H. 2024. Differentiating Through Integer Linear Programs with Quadratic Regularization and Davis-Yin Splitting. *Transactions on Machine Learning Research*.
- Munch, E. 2017. A User’s Guide to Topological Data Analysis. *Journal of Learning Analytics*, 4(2): 47–61.
- OpenAI. 2024. Learning to Reason with LLMs. Accessed: 2025-04-27.
- Perea, J. A.; and Harer, J. 2015. Sliding Windows and Persistence: An Application of Topological Methods to Signal Analysis. *Foundations of Computational Mathematics*, 15: 799–838.
- Ramzi, Z.; Mannel, F.; Bai, S.; Starck, J.-L.; Ciuciu, P.; and Moreau, T. 2022. SHINE: SHaring the INverse Estimate from the forward pass for bi-level optimization and implicit models. In *ICLR 2022-International Conference on Learning Representations*.
- Rolf, E.; Worledge, T. T.; Recht, B.; and Jordan, M. 2021. Representation Matters: Assessing the Importance of Subgroup Allocations in Training Data. In Meila, M.; and Zhang, T., eds., *Proceedings of the 38th International Conference on Machine Learning*, volume 139 of *Proceedings of Machine Learning Research*, 9040–9051. PMLR.
- Schwarzschild, A.; Borgnia, E.; Gupta, A.; Bansal, A.; Emam, Z.; Huang, F.; Goldblum, M.; and Goldstein, T. 2021a. Datasets for Studying Generalization from Easy to Hard Examples.
- Schwarzschild, A.; Borgnia, E.; Gupta, A.; Huang, F.; Vishkin, U.; Goldblum, M.; and Goldstein, T. 2021b. Can You Learn an Algorithm? Generalizing from Easy to Hard Problems with Recurrent Networks. *Advances in Neural Information Processing Systems*, 34: 6695–6706.
- Schwarzschild, A.; Gupta, A.; Goldblum, M.; and Goldstein, T. 2021c. Thinking Deeply with Recurrence: Generalizing from Easy to Hard Sequential Reasoning Problems. *CoRR*.



Schwarzschild, A.; McLeish, S. M.; Bansal, A.; Diaz, G.; Stein, A.; Chandnani, A.; Saha, A.; Baraniuk, R.; Tran-Thanh, L.; Geiping, J.; et al. 2023. Algorithm Design for Learned Algorithms.

Shah, R.; Varma, V.; Kumar, R.; Phuong, M.; Krakovna, V.; Uesato, J.; and Kenton, Z. 2022. Goal Misgeneralization: Why Correct Specifications Aren’t Enough For Correct Goals. arXiv:2210.01790.

Takens, F. 2006. Detecting strange attractors in turbulence. In *Dynamical Systems and Turbulence, Warwick 1980: proceedings of a symposium held at the University of Warwick 1979/80*, 366–381. Springer.

Tralie, C. J.; and Perea, J. A. 2018. (Quasi)Periodicity Quantification in Video Data, Using Topology. *SIAM Journal on Imaging Sciences*, 11(2): 1049–1077.

Veličković, P.; Badia, A. P.; Budden, D.; Pascanu, R.; Banino, A.; Dashevskiy, M.; Hadsell, R.; and Blundell, C. 2022. The clrs algorithmic reasoning benchmark. In *International Conference on Machine Learning*, 22084–22102. PMLR.

Winston, E.; and Kolter, J. Z. 2020. Monotone operator equilibrium networks. *Advances in neural information processing systems*, 33: 10718–10728.

Wu Fung, S.; Heaton, H.; Li, Q.; McKenzie, D.; Osher, S.; and Yin, W. 2022. JFB: Jacobian-Free Backpropagation for Implicit Networks. In *Proceedings of the AAAI Conference on Artificial Intelligence*, volume 36, 6648–6656.

Yin, W.; McKenzie, D.; and Fung, S. W. 2022. Learning to Optimize: Where Deep Learning Meets Optimization and Inverse Problems. *SIAM News*.

## A Additional Maze Dataset Details

Both DT-Net and PI-Net were trained on the same maze dataset (Schwarzschild et al. 2021a) containing 50,000 mazes of size  $9 \times 9$ , meaning the mazes are subgraphs of the  $5 \times 5$  lattice. Training mazes were generated via RDFS without percolation, and with the start position being constrained to being at a dead end (exactly 1 neighbor). We mimic this training distribution and add out-of-distribution shifts using the `maze-dataset` Python package (Ivanitskiy et al. 2023b).

We first note that for controlling maze size, `maze-dataset.MazeDatasetConfig` takes a parameter `grid_n`, which denotes the size of the lattice subgraph. By contrast, the “easy to hard” (Schwarzschild et al. 2021a) dataset considers an  $n \times n$  maze in its raster representation. To convert between these two notions of maze size, we set

$$n = 2 \cdot \text{grid\_n} - 1.$$

We can modify the start position constraint in `maze-dataset` by setting `deadend_start=False` in `endpoint_kwargs`. When `False`, the start position is sampled uniformly at random from all valid nodes, while when `True` the start position is samples uniformly at random from all valid nodes with degree one. Valid nodes are, by default, those not directly matching the end position or directly adjacent to it.

Randomized depth-first search (RDFS) is a standard algorithm for generating mazes, and produces mazes which are spanning trees of the underlying lattice, and thus do not contain cycles. For any acyclic graph with a

spanning connected component, there is a unique (non-backtracking) path between any pair of points, and thus solutions are guaranteed to be unique. In our work, we select `LatticeMazeGenerators.gen_dfs_percolation` as the `maze_ctor` parameter. This function takes an additional variable `p` in `maze_ctor_kwargs`, which controls the percolation parameter. This percolation parameter, denoted  $p$  in our work, means that the final maze is the result of a logical OR operation on the presence of all possible edges in the maze between an initial maze generated via RDFS and a maze generated via percolation, where each edge is set to exist with probability  $p$ . This is equivalent to first generating a maze with RDFS and then setting each wall to an edge with probability  $p$ . Since the initial RDFS maze is a spanning tree, adding any edge will cause the creation of a cycle, thus giving our desired out-of-distribution mazes.

## B Topological Data Analysis

Topological Data Analysis, or TDA, attempts to produce informative summaries of high dimensional data, typically thought of as point clouds<sup>7</sup>  $\mathcal{U} = \{u_1, \dots, u_K\} \subset \mathbb{R}^n$ , by adapting tools from algebraic topology.

### B.1 Simplicial Complexes

We are interested in TDA tools based on the idea of homology groups (Hatcher 2002, Chapter 2). Homology groups can be computed algorithmically from a geometric object known as a *simplicial complex*, which we define below.

**Definition 1.** We collect definitions of several relevant concepts related to simplices.

1. A  $k$ -simplex is the convex hull of any  $k + 1$  points in  $\mathbb{R}^k$ ,

$$\begin{aligned} \sigma &:= \text{Conv} \{u_1, \dots, u_{k+1}\} \\ &= \left\{ \sum_{i=1}^{k+1} \alpha_i u_i : \alpha_i \geq 0 \text{ and } \sum_{i=1}^{k+1} \alpha_i = 1 \right\} \end{aligned} \quad (3)$$

2. A face of a  $k$ -simplex  $\sigma$  is a piece of the boundary of  $\sigma$  which is itself a simplex. That is,  $\tau$  is a face of  $\sigma$  defined in (3) if

$$\tau = \text{Conv} \{u_{i_1}, \dots, u_{i_{\ell+1}}\}$$

3. A simplicial complex  $\mathcal{S}$  is a set of simplices, of multiple dimensions, satisfying the following properties
  - (a) For all  $\sigma \in \mathcal{S}$ , all faces of  $\sigma$  are also in  $\mathcal{S}$ .
  - (b) If any two  $\sigma_1, \sigma_2 \in \mathcal{S}$  have non-empty intersection, then  $\sigma_1 \cap \sigma_2$  is a face of both  $\sigma_1$  and  $\sigma_2$ , and consequently  $\sigma_1 \cap \sigma_2 \in \mathcal{S}$ .

The process of computing homology groups from a simplicial complex is beyond the scope of this paper. We refer the reader to (Hatcher 2002, Chapter 2) for further details. It is also possible to define homology groups for *abstract simplicial complexes*,  $\mathcal{R}$ , for which a  $k$ -simplex  $\sigma \in \mathcal{R}$  is not literally a convex hull, but merely a list of points:

$$\sigma = \{u_1, \dots, u_{k+1}\}. \quad (4)$$

<sup>7</sup>By using the term “point cloud” we are implying that the ordering of points does not matter.

In this case, a face is just a subset of  $\sigma$ :

$$\tau = \{u_{i_1}, \dots, u_{i_{\ell+1}}\}. \quad (5)$$

Note that condition 3 (b) of Appendix Definition 1 is now vacuously true.

## B.2 Homology Groups

Although we have not stated exactly how homology groups are defined, in this section we discuss a few of their properties. Fix a (possibly abstract) simplicial complex  $\mathcal{S}$ . We shall work with homology groups with coefficients in the field  $\mathbb{Z}_2 := \mathbb{Z}/2\mathbb{Z}$ , hence all homology groups will be vector spaces over  $\mathbb{Z}_2$ . We will focus on the zeroth and first homology groups, denoted  $H_0(\mathcal{S})$  and  $H_1(\mathcal{S})$  respectively. Elements in  $H_0(\mathcal{S})$  are equivalence classes of points, where two points are equivalent if they are in the same path component of  $\mathcal{S}$ . Elements in  $H_1(\mathcal{S})$  are equivalence classes of closed loops, where two loops are equivalent if they “encircle the same hole” (Munch 2017). Consequently, the dimension of  $H_0(\mathcal{S})$  (the zeroth *Betti number*,  $B_0(\mathcal{S})$ ) counts the number of path connected components of  $\mathcal{S}$ , while the dimension of  $H_1(\mathcal{S})$  (the first *Betti number*,  $B_1(\mathcal{S})$ ) counts the number of distinct holes in  $\mathcal{S}$ .

## B.3 The Rips Complex

Given the above, in order to associate Betti numbers to a point cloud we first need to define an appropriate simplicial complex.

**Definition 2** (The Vietoris-Rips complex). Fix a point cloud  $\mathcal{U} = \{u_1, \dots, u_K\} \subset \mathbb{R}^n$ , and for simplicity assume that  $K < n$ . Select a distance parameter  $\epsilon \geq 0$ . We define the simplicial complex  $\mathcal{S}_\epsilon$ , known as the Vietoris-Rips, or simply Rips, complex to contain all simplices

$$\sigma = \text{Conv} \{u_{i_1}, \dots, u_{i_{\ell+1}}\}, \quad (6)$$

satisfying the condition:

$$\max_{1 \leq m < n \leq \ell+1} \|u_{i_m} - u_{i_n}\|_2 \leq \epsilon. \quad (7)$$

In words,  $\mathcal{S}_\epsilon$  contains all simplices on  $\mathcal{U}$  with a diameter less than  $\epsilon$ . We note that  $\mathcal{S}_0 = \mathcal{U}$  and hence  $B_0(\mathcal{S}_0) = |\mathcal{U}|$ , as every point in  $\mathcal{U}$  is its own connected component., while  $B_1(\mathcal{S}_0) = 0$ . On the other end of the scale, when  $\epsilon > \text{diam}(\mathcal{U})$ , where

$$\text{diam}(\mathcal{U}) = \max_{1 \leq i < j \leq N} \|u_i - u_j\|_2, \quad (8)$$

the full-dimensional simplex

$$\sigma = \text{Conv} \{u_1, \dots, u_K\} \quad (9)$$

is contained in  $\mathcal{S}_\epsilon$ , and thus  $\mathcal{S}_\epsilon$  has one connected component and no loops:  $B_0(\mathcal{S}_\epsilon) = 1$ ,  $B_1(\mathcal{S}_\epsilon) = 0$ . Consequently, the important topological features of  $\mathcal{U}$  are detected by the Rips complex for  $\epsilon$  values in  $(0, \text{diam}(\mathcal{U}))$ .

The condition  $K < n$  in Appendix Definition 2 may be removed, in which case  $\mathcal{S}_\epsilon$  is defined as an abstract simplicial complex. This distinction is not relevant for our work.

## B.4 Persistent Betti Numbers

Which value of  $\epsilon$  should one choose? As discussed in Munch (2017), the trick is not to select a particular value of  $\epsilon$  but rather focus on features (concretely: equivalence classes in  $H_0(\mathcal{S}_\epsilon)$  and  $H_1(\mathcal{S}_\epsilon)$ ) which *persist* for large ranges of  $\epsilon$ . More specifically, we define  $\epsilon_b$ , the *birth time*, to be the value of  $\epsilon$  at which a particular equivalence class is first detected in  $\mathcal{S}_\epsilon$ . The death time,  $\epsilon_d$ , is the largest value of  $\epsilon$  for which a particular equivalence class is detected in  $\mathcal{S}_\epsilon$ . Fixing a threshold `thresh`, we say an equivalence class is *persistent* if  $\epsilon_d - \epsilon_b > \text{thresh}$ . We define the persistent zeroth (respectively first) Betti number  $B_0$  (respectively  $B_1$ ) to be the number of distinct equivalence classes appearing in  $H_0(\mathcal{S}_\epsilon)$  (respectively  $H_1(\mathcal{S}_\epsilon)$ ) which satisfy  $\epsilon_d - \epsilon_b > \text{thresh}$ .

## B.5 Sliding Window Embedding

Finally, we note that Perea and Harer (2015); Tralie and Perea (2018) propose a more sophisticated method for detecting periodicity using the *sliding window embedding*, also known as the *delay embedding*:

$$\{u_j\}_{j=1}^K \mapsto \left\{ SW_{d,\tau}(u_j) := \begin{bmatrix} u_j \\ u_{j+\tau} \\ \vdots \\ u_{j+d\tau} \end{bmatrix} \right\}_{j=1}^{K-d\tau}, \quad (10)$$

where  $\tau$  (the delay) and  $d$  (the window size) are user-specified parameters. Then, persistent Betti numbers are computed for  $\{SW_{d,\tau}(u_j)\}_{j=1}^{K-d\tau}$  instead. This construction is motivated by Taken’s theorem (Takens 2006) which, informally speaking, states that the dynamics of  $\{u_j\}_{j=1}^K$  can be recovered completely from its sliding window embedding, for sufficiently large  $d$ . Note this comes at a price: the increase in dimension means an increase in computational cost.

In preliminary experiments we found that the persistent Betti numbers for  $\{SW_{d,\tau}(u_j)\}_{j=1}^{K-d\tau}$  did not reveal anything that could not already be inferred from the persistent Betti numbers of  $\{u_j\}_{j=1}^K$ . Thus, we chose not to work with the sliding window embedding.

## C Additional Experimental Details

### C.1 Models Summary

### C.2 Training Details

For each model type, many variations of hyperparameters such as learning rate, gradient clipping, contractivity, tolerance, warmup, Jacobian-free backpropagation (Wu Fung et al. 2022), and others were explored, and the best-performing models were selected to serve as representative examples. The training runs in Section 4 all utilized a 90/10 training/validation split of 100k mazes over 100 epochs, learning rate of  $10^{-4}$ , AdamW optimizer, and ReduceLRonPlateau learning rate scheduler with patience 10 and reduction factor 0.1. DT-Net was trained with gradient clip of 1.0 and progressive loss from (Bansal et al. 2022) with  $\alpha = 0.01$ . IT-Net was trained without gradient clipping, maximum iterations 100 with convergence tolerance 0.1, and using Jacobian-free backpropagation (Wu Fung et al.

Table 2: Summary of models used in experiments.

Model	Description	Params (M)	Size (MB)	Trained by
FF-Net	fully-convolutional feedforward	8.89	33.91	Us
PI-Net	INN	0.78	2.99	Anil et al. (Anil et al. 2022)
DT-Net	weight-tied, input-injected RNN	0.78	2.99	Bansal et al. (Bansal et al. 2022) and Us
IT-Net	INN variant of DT-Net	1.37	5.24	Us

2022). See the code provided in the supplemental material for full details.

### C.3 Additional Details on PI-Net

During our experiments we determined that there was another model parameter, beyond the number of iterations, that had a strong impact on the accuracy of PI-Net. Specifically, there is a `threshold` parameter within the forward solver, Broyden’s method, that controls the maximum rank of the inverse Jacobian approximation. Based on code included in the supplementary material for Anil et al. (2022), it appears the `threshold` parameter was originally set at 40. However, with this setting PI-Net performed very poorly; it failed on all mazes of size  $49 \times 49$ . Increasing `threshold` increased the accuracy of PI-Net, but also increases memory costs because it requires storing a number of high-dimensional latent iterates equal to `threshold`. For our experiments, we used `threshold = 1,000` in order to achieve strong accuracy without unreasonable memory requirements.

### C.4 Computational Resources

The experiments in this study were performed on a high-performance workstation with the following specifications:

- **CPU:** AMD Ryzen Threadripper PRO 3955WX (16 cores, 32 threads)
- **GPU:** 3x NVIDIA RTX A6000 (48 GiB VRAM)
  - CUDA Version: 12.5, Driver Version: 555.42.06
- **Memory:** 251 GiB RAM
- **Operating System:** Ubuntu 20.04.6 LTS (x86\_64 architecture)

as well as a node of a High Performance Computing platform with the following specifications:

- **CPU:** AMD EPYC 9534 (64 cores, 128 threads)
- **GPU:** 4x NVIDIA RTX A6000 (48 GiB VRAM)
- **Memory:** 768 GiB RAM
- **Operating System:** Ubuntu 20.04.6 LTS Server.

Testing of two pre-trained models in Section 3 took about 40 GPU hrs per model or 80 GPU hours total. Training of the models in Section 4 took about 10 GPU hours per model and training distribution pair, or about 180 GPU hours total. The full research project required much more compute due to hundreds of GPU hours spent on hyperparameter selection. The final hyperparameters used in experiments are provided in the supplemental material.

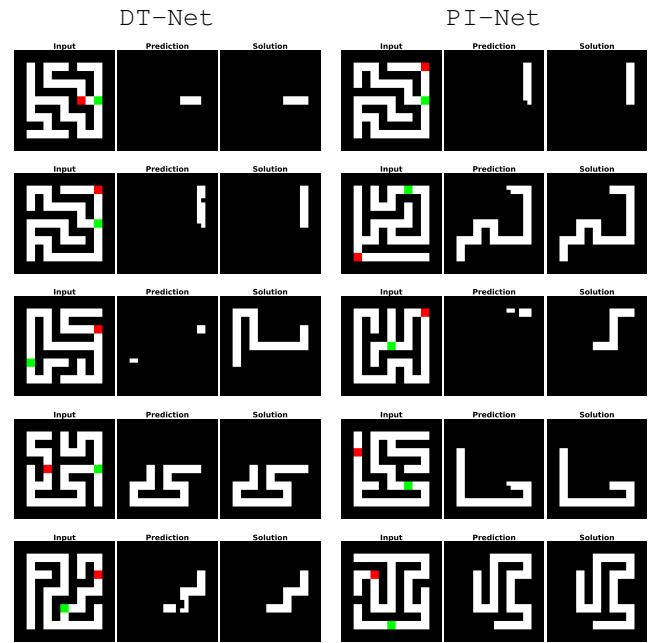


Figure 10: Examples of  $9 \times 9$  mazes with `deadend_start=False` predictions from DT-Net (left) and PI-Net (right), some of which they fail to solve. Note that mistakes are often in the start position cell or cells immediately adjacent to it.

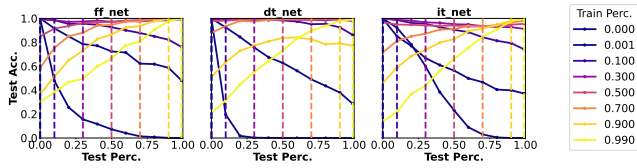


Figure 11: Alternative visualizations of test accuracy for FF-Net, DT-Net, and IT-Net across different test percolation values at maze size 9 (the training maze size). Each accuracy value is computed from a sample of 1000 test mazes. The dashed vertical lines illustrate the training percolation value of the model with the matching color.

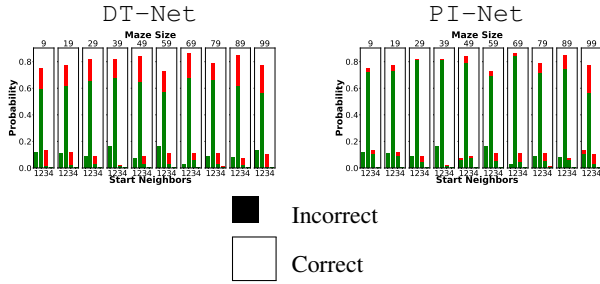


Figure 12: DT-Net and PI-Net predictions for `deadend_start=False` mazes, split by maze size and number of start-node neighbors. Accuracy drops as neighbor-count rises.

## D Additional Experimental Results

### D.1 Failed Model Predictions

### D.2 Additional Experimental Results

Figure 11 provides an alternative visualization of the test accuracy for the models of Section 4, while Figure 12 breaks down test accuracy by start node degree, when `deadend_start` is set to `True`.

## E The Ripser Wrapper

A number of optimizations were applied to reduce the memory and compute time of TDA. Instead of providing

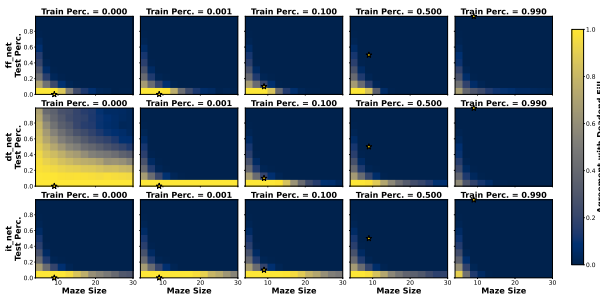


Figure 13: Heatmap showing the agreement between the trained-from-scratch instances of FF-Net, DT-Net, and IT-Net with the deadend-fill algorithm, across various maze sizes and test percolation values.

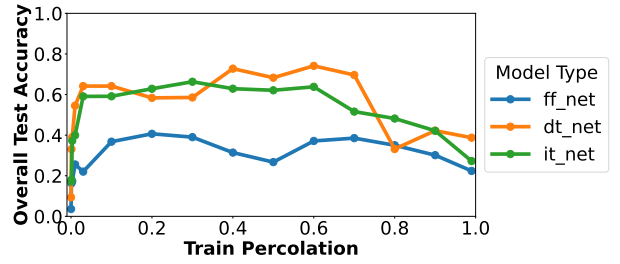


Figure 14: Plots of overall test accuracy (average accuracy over all test mazes) as a function of train percolation for DT-Net, IT-Net, and FF-Net. Each point is a trained model.

a sequence of high-dimensional latent iterates directly to Ripser, we use a smaller distance matrix containing pairwise distances between the iterates. This matrix is computed using an optimization from Tralie and Perea (2018), where the iterates are first compressed with singular value decomposition (SVD) to reduce memory costs. The SVD computation is performed in `PyTorch` to leverage GPU acceleration. Initially, we also used a diagonal convolution optimization, also from Tralie and Perea (2018), to avoid redundant computations when constructing the distance matrix for the sliding window embedding. However, this second optimization was not used in our final TDA experiments, as we dropped the sliding window embedding.